Transient frequency responses for pressurized water pipelines containing blockages with linearly varying diameters

T. C. Che [1]; **H. F. Duan** [2], *M.ASCE*; **P. J. Lee** [3]; **B. Pan** [4]; **M. S. Ghidaoui** [5], *M.ASCE*

[1] Ph.D. Student, Department of Civil and Environmental Engineering, The Hong Kong Polytechnic University, Hung Hom, Kowloon, Hong Kong SAR, PR China. E-mail: tong-chuan.che@connect.polyu.hk

[2] Assistant Professor, Department of Civil and Environmental Engineering, The Hong Kong Polytechnic University, Hung Hom, Kowloon, Hong Kong SAR, PR China. E-mail: hf.duan@polyu.edu.hk

[3] Professor, Department of Civil and Natural Resources Engineering, The University of Canterbury, Private Bag 4800, Christchurch, New Zealand. E-mail: pedro.lee@canterbury.ac.nz

[4] Ph.D. Student, Department of Civil and Environmental Engineering, The Hong Kong Polytechnic University, Hung Hom, Kowloon, Hong Kong SAR, PR China. E-mail: bin.pan@connect.polyu.hk

[5] Chair Professor, Department of Civil and Environmental Engineering, The Hong Kong University of Science and Technology, Kowloon, Hong Kong SAR, PR China. E-mail: ghidaoui@ust.hk

Abstract

Extended partial blockages in urban water supply systems (UWSS) are formed from complicated physical, chemical, and biological processes, thus these blockages are commonly in random and non-uniform geometries. The transient-based blockage detection method (TBBDM) has been evidenced in many applications to be a promising way to diagnose these blockages. Despite the successful validation and application of the TBBDM in the literature, pipe blockages used in these studies were idealized and simplified to regular and uniform shape, which are however not common in practical UWSS, and thus invalidity and inaccuracy of this TBBDM has been widely observed in practical applications. This paper presents a fundamental research on understanding the influence of more realistic and non-uniform blockages on transient wave behavior and the accuracy of current TBBDM. The blockage with a linearly varying diameter (termed as non-uniform blockage) is firstly investigated by the frequency domain analytical analysis for its impact on transient wave behavior, which is thereafter incorporated in the overall transfer matrix of transient frequency response for reservoir-pipeline-valve systems. The results indicate the non-uniform blockage may induce very different modification patterns on the frequency shift and amplitude change of transient waves from the uniform blockage situation.

Keywords: Non-uniform blockage; Water pipelines; Transient; Frequency response; Transfer matrix

Introduction

Blockages are commonly existed in pressurized fresh water and seawater conveying pipelines due to various physical, chemical, and biological processes, including corrosion, biofilm accumulation, and deposition of sediments. Blockages can reduce pipe diameters and increase pipe wall roughness, resulting in lower water carrying capacity, additional energy loss and deterioration of water quality (James & Shahzad, 2003). Unlike leaks, blockages are masked in the inaccessible buried pipeline network since they lack external evidence needed for detection and the lost pressure and flow across the blockage can be compensated by other branch pipelines in the network (Stephens, 2008). Therefore, it is crucial to develop a non-destructive blockage detection method to reduce the impact of blockages on the urban water supply systems (UWSS).

A variety of pipeline fault (leakage and blockage) detection methods has been summarized by Datta and Sarkar (2016), among which the transient-based method (Colombo et al., 2009; Lee et al., 2013) is thought to be a promising way for diagnosing pipeline faults because it has the desirable merits of high efficiency, low cost, and non-destructive applications. The principle of this method is that pipeline faults can be detected by inducing a transient pressure wave into the pipeline followed by measuring and analyzing the pressure wave echoes (transient responses) from the potential pipe faults. Localized pipe faults (such as leaks and discrete blockages) generate additional pressure signals within the transient response, therefore the location of these localized faults can be determined based on the occurrence time of the first pressure signal and the system wave speed. The transient-based analysis approach has been developed and used by many researchers for detecting and locating different localized pipe faults in the time domain (Brunone, 1999; Brunone & Ferrante, 2001; Covas & Ramos, 2010; Covas et al., 2004; Lee et al., 2007; Meniconi et al., 2010, 2011). Though it is easy to

operate, the small reflected pressure signal from localized faults is easily interfered by random background noise, making it difficult to accurately identify. Moreover, the complexity of system connections (such as multiple-pipe systems) may cause technical trouble for separating the transient response information (e.g., reflection) of faults from other sources when using this time-domain method. To address this problem, a number of publications proposed spectral analysis as an alternative way for detecting and sizing different localized faults in the frequency domain (Brunone & Ferrante, 2004; Ferrante & Brunone, 2003; Gong et al., 2014; Kim, 2017; Lee et al., 2006, 2008a, 2015; Sattar & Chaudhry, 2008; Wang et al., 2005).

Specifically, Lee et al. (2006) showed that the presence of leak in pipeline induces a sinusoidal fluctuation pattern (termed the leak-induced pattern) onto the resonance peaks, and the amplitude and shape of this leak-induced pattern can be used to detect the size and location of leak. It was also found that resonance peaks of leak case are in the same position as the leak-free case, in other words no shifting of the frequency peaks are imposed. Discrete blockages in pipelines were found to have a similar influence on the resonant peaks (Lee et al., 2008a; Sattar et al., 2008), therefore the size and location of discrete blockage can be diagnosed using a similar approach. Brunone et al. (2008) showed that extended blockages, which is a common scenario in aging pipelines, have a totally different influence on transient responses from discrete blockages, and thus methods used for discrete blockage detection may not be applicable to extended blockages. Duan et al. (2012) showed that extended blockages not only change the amplitude of resonant peaks, but also induce frequency shifts in resonant peaks (termed as blockage-induced frequency shifts). On the basis of the derived wave-blockage dispersion relationship in Duan et al. (2012), a genetic algorithm (GA) based inverse optimization procedure was proposed to determine the physical properties (such as length, size and

location) of potential extended blockages. Duan et al. (2014) further inspected the transient wave-blockage interaction and theoretically explained the above-mentioned blockage-induced frequency shifts.

Despite the successful application of this transient-based method for extended blockage detection in many numerical and laboratory tests, blockages used for analysis in previous studies were idealized and simplified to uniform shape (Duan et al., 2012, 2014; Lee et al., 2013; Louati et al., 2017; Meniconi et al., 2013; Rubio Scola et al., 2017; Tuck et al., 2013), which are actually equivalent to multiple pipe sections in series with different diameters connected together. However, real world blockages that are often formed from complex sources and processes are usually in highly random and non-uniform shape as illustrated in Figs. 1(a) and 1(b). Recently, Duan et al. (2017) experimentally investigated the influence of non-uniform blockages on transient wave behavior and the validity of current transient-based method for non-uniform blockage detection. It has been found that the blockage non-uniformity may have a great impact on both the wave attenuation and the phase (frequency) shift, which causes invalidity and inaccuracy of the current transient-based method when it is used to detect these non-uniform blockages. Therefore, a further and in-depth understanding of the influence of non-uniform blockages on transient responses is important for the development of more accurate blockage detection method for practical UWSS.

To study the modification effect of non-uniform blockages on the system frequency response, Chaudhry (2014) replaced the actual non-uniform blockage (i.e., pipeline with gradually varying diameter) by a number of substitute uniform blockages in series. This treatment discretized the non-uniform blockage into many pricewise constant elements, and then individual matrixes for each element are multiplied to produce the approximated overall matrix for the whole non-uniform

blockage. From their results, this approximation method only gives satisfactory prediction for the first few harmonic modes, and it is computationally expensive to get relatively accurate results for higher harmonic modes. As a result, this approximation treatment method may induce potential errors and influences for the transient modeling and utilization such as pipe blockage detection, especially for the pipeline with multiple blockages (Duan et al., 2010). Therefore, it is worthwhile to develop more reliable (more accurate and efficient) methods to describe the transient frequency response of realistic blockage situations in water pipelines.

As a preliminary study, it is preferable and feasible to examine the realistic cases of non-uniform blockages by starting with simple cases, such as blockages with linearly varying diameters (termed as non-uniform blockages in this study) as shown in Fig. 1(c), with the aim to understand the fundamental physics and mechanism of wave-blockage interactions. Specifically, the transient wave behavior in a single non-uniform blockage is obtained by analytically solving the wave equation under specific initial and boundary conditions. Thereafter, the obtained wave solutions are used to derive the overall transfer matrix for water pipeline systems with non-uniform blockages. The derived transfer matrix is fully validated by the traditional method of characteristics (MOC), and then used to systematically investigate the influences of non-uniform blockage shape, severity, and length on transient frequency responses. Finally, the findings and practical implications of this study are discussed.

Models and Methods

Wave equation for a single non-uniform blockage

The one-dimensional (1D) wave equation for non-uniform blockages with varying cross-sectional

areas was derived as (Duan et al., 2011; Duan, 2017)

$$A\frac{\partial^2 P}{\partial t^2} = a^2 \frac{\partial}{\partial x}\left(A\frac{\partial P}{\partial x} \right). \tag{1}$$

where t = time; x = axial coordinate along the pipeline; $A = A(x)$ = pipe cross-sectional area; P = instantaneous pressure in the time domain; $a = a(x)$ = acoustic wave speed, which represents the characteristics of pipe-wall deformation and properties of internal fluid (e.g., water).

Note that a frictionless pipeline system with elastic pipe wall is firstly considered in the analytical derivation to highlight the wave-blockage interaction (Duan et al., 2014). Pipeline systems with linearized steady friction will be further discussed in the numerical applications.

Alternatively, Eq. (1) can be rewritten as

$$\frac{\partial^2 P}{\partial t^2} - a^2 \frac{\partial^2 P}{\partial x^2} = a^2 \frac{A'}{A}\frac{\partial P}{\partial x}, \tag{2}$$

where A' = the derivative dA/dx. For transient pipe flows, the instantaneous pressure P can be expressed as (Chaudhry, 2014)

$$P = P_0 + p^*, \tag{3}$$

where P_0 = mean pressure; p^* = pressure deviation from the mean. Because the pipeline is frictionless, P_0 is constant in terms of both x and t, then Eq. (2) becomes

$$\frac{\partial^2 p^*}{\partial t^2} - a^2 \frac{\partial^2 p^*}{\partial x^2} = a^2 \frac{A'}{A}\frac{\partial p^*}{\partial x}, \tag{4}$$

which is a linear partial differential equation (PDE), and can be solved under specific boundary and initial conditions.

Transient wave behavior in a single non-uniform blockage

In above wave equation, it is assumed that the solution p^* has the following form (Chaudhry, 2014)

$$p^*(x,t) = p(x)e^{i\omega t}, \tag{5}$$

where p = pressure in the frequency domain; ω = angular frequency; i = imaginary part.

Substituting Eq. (5) back into Eq. (4), the PDE becomes the following linear ordinary differential equation (ODE)

$$\frac{d^2 p}{dx^2} + \frac{A'}{A}\frac{dp}{dx} + k^2 p = 0, \tag{6}$$

where $k = k(x) = \omega/a(x)$ = wave number. In fact, Eq. (6) is in the same form with the Webster's horn equation in acoustics (Webster, 1919). The variation of the wave speed within a shallow non-uniform blockage along the axial direction is relatively small compared with the wave speed a_0 in intact sections. For example, the field tests by Lee et al. (2017) showed that the average percentage of wave speed variation in deteriorated field water pipelines is around 8.25%. Thus, the wave speed $a_b(x)$ within the non-uniform blockage is represented by the average value (i.e., $\bar{a}_b$) throughout the blockage section, which is different from the original value of intact pipelines (i.e., a_0) because of the blockage-induced changes in pipe properties (e.g., diameter, thickness and material). As a result, the wave number k within the non-uniform blockage in Eq. (6) becomes $k_b = \omega/\bar{a}_b$. Sensitivity analysis will be conducted later in this paper to examine the validity range (limitation) of this assumption (i.e., using the average wave speed within the blockage section).

Applying Eq. (6) in the n-th non-uniform blockage, as shown in Fig. 1(c), provides

$$\frac{d^2 p_n}{dx^2} + \frac{A_n'}{A_n}\frac{dp_n}{dx} + k_b^2 p_n = 0. \tag{7}$$

For analytical analysis, the pipe radius of the n-th non-uniform blockage in Fig. 1(c) is defined as

$$r_n(x) = s_n x + R_{Ln}, \tag{8}$$

where r_n = pipe radius of the n-th non-uniform blockage; R_{Ln} = pipe radius at the left boundary of the n-th non-uniform blockage; $s_n = (R - R_{Ln})/l_n$ = slope of the n-th non-uniform blockage, in which R = intact pipe radius and l_n = length of the n-th non-uniform blockage in Fig. 1(c).

176 Based on the expression of r_n in Eq. (8), the pipe cross-sectional area A_n and its derivative A_n' can

177 be calculated, thus

178 $$\frac{A_n'(x)}{A_n(x)} = \frac{2s_n}{s_n x + R_{Ln}}. \tag{9}$$

179 Substituting Eq. (9) into Eq. (7), it becomes

180 $$\frac{d^2 p_n}{dx^2} + \frac{2s_n}{s_n x + R_{Ln}} \frac{dp_n}{dx} + k_b^2 p_n = 0. \tag{10}$$

181 It is assumed that the solution for the wave equation Eq. (10) is a plane wave solution in the following

182 form (Munjal, 2014)

183 $$p_n = \frac{e^{\alpha x}}{r_n(x)} = \frac{e^{\alpha x}}{s_n x + R_{Ln}}, \tag{11}$$

184 where α = coefficient that remains to be determined; note that the denominator is the pipe radius of

185 the n-th non-uniform blockage in Eq. (8). Furthermore, substituting Eq. (11) into Eq. (10) results in

186 the following characteristic equation for α

187 $$\alpha^2 + k_b^2 = 0. \tag{12}$$

188 As a result, α has two solutions

189 $$\alpha_1 = ik_b, \quad \alpha_2 = -ik_b. \tag{13}$$

190 Substituting two solutions into Eq. (11), two special solutions for wave equation Eq. (10) can be

191 obtained

192 $$(p_n)_1 = \frac{e^{ik_b x}}{s_n x + R_{Ln}}, \quad (p_n)_2 = \frac{e^{-ik_b x}}{s_n x + R_{Ln}}. \tag{14}$$

193 In fact, these two plane wave solutions $(p_n)_1$ and $(p_n)_2$ are the incident and reflected waves propagating

194 towards opposite directions. It can be observed from the numerator of Eq. (14) that the transient

195 waves distribute sinusoidally in space with a constant wave number k_b. In addition, the amplitude of

196 these two waves is modified by the denominator, which is the pipe radius of the *n*-th non-uniform
197 blockage. It means that the wave amplitude is inversely proportional to the radius of the *n*-th
198 non-uniform blockage.

199 Because the wave equation Eq. (10) is a linear ODE, based on the superposition principle, the
200 general solution for wave equation can be obtained

201 $$p_n = \frac{C_1 e^{ik_b x} + C_2 e^{-ik_b x}}{s_n x + R_{Ln}}, \tag{15}$$

202 where C_1 and C_2 are two constants.

203 To have an intuitive sense of wave behavior in a single non-uniform blockage, the plane wave
204 solutions in Eq. (14) are visualized in both uniform and non-uniform blockages. A localized incident
205 wave is created at the right boundary of these two blocked pipelines, and detailed parameters of these
206 two systems are listed in Table 1. Note that these two pipelines have the same blocked volume, which
207 means that the average pipe diameter for these two blockages is the same, and the left boundaries of
208 these two pipelines are reflection-free. The obtained results are plotted in Fig. 2, showing how the
209 localized incident wave evolves as it propagates in the pipeline from right to left. The spatial
210 coordinate x is normalized by the intact pipe radius R, and is expressed as x_D in the horizontal axis.
211 The pressure is normalized by the pressure in the intact pipeline, and is expressed as dimensionless
212 pressure p_D.

213 It can be seen from Fig. 2 that the wave amplitude in the uniform blockage keeps constant, while
214 the wave amplitude in the non-uniform blockage gradually increases as the wave propagates to the left.
215 This is consistent with the wave solution in Eq. (14), because the denominator of Eq. (14) for the
216 non-uniform blockage gradually decreases from right to left. In fact, this result is consistent with the
217 former study by the authors with regard to energy analysis of wave scattering in disordered-diameter

pipelines (Duan et al., 2011). That is, non-uniform blockages in the pipeline may cause the energy re-distribution of pressure waves in both temporal and spatial domains in the system.

Overall transfer matrix for pipeline systems with a single non-uniform blockage

To study the transient frequency responses for pipeline systems with a single non-uniform blockage, the obtained wave solution in Eq. (15) is used to derive the transfer matrix. The transfer matrix is the linearized counterpart of mass and momentum equations in the frequency domain. It describes the wave behavior and connects state vectors at two boundaries of the pipeline system without discretization of the pipeline in space. Thus, it has the advantage of computational efficiency compared with some time domain methods, such as the MOC.

The derivation procedure of the transfer matrix for a single uniform blockage (or pipeline) was provided in Chaudhry (2014). A similar procedure is adopted herein to derive the transfer matrix for a single non-uniform blockage, based on the wave solution in Eq. (15). Note that the pressure deviation p in Eq. (15) is transformed into the pressure head deviation h in this section, which is a common practice in hydraulic engineering.

The derived transfer matrix for a single non-uniform blockage (i.e., the n-th non-uniform blockage in Fig. 1(c)) is

$$\begin{pmatrix} q \\ h \end{pmatrix}_{n+1} = \begin{pmatrix} U_{11} & U_{12} \\ U_{21} & U_{22} \end{pmatrix} \begin{pmatrix} q \\ h \end{pmatrix}_{n}, \tag{16}$$

where q = discharge deviation in the frequency domain; h = pressure head deviation in the frequency domain; subscript n and n+1 are upstream and downstream boundaries of the n-th non-uniform blockage, respectively; U_{ij} = elements of transfer matrix, with the following forms:

$$U_{11} = -\frac{iR_{Ln}}{2k_b\left(s_n l_n + R_{Ln}\right)^2}\frac{A_{n+1}}{A_n}\left\{\left[ik_b\left(s_n l_n + R_{Ln}\right) - s_n\right]e^{ik_b l_n} + \left[ik_b\left(s_n l_n + R_{Ln}\right) + s_n\right]e^{-ik_b l_n}\right\};$$

$$U_{12} = \frac{A_{n+1}g}{2\omega k_b\left(s_n l_n + R_{Ln}\right)^2}\left\{\left[ik_b\left(s_n l_n + R_{Ln}\right) - s_n\right]\left(ik_b R_{Ln} + s_n\right)e^{ik_b l_n} - \left[ik_b\left(s_n l_n + R_{Ln}\right) + s_n\right]\left(ik_b R_{Ln} - s_n\right)e^{-ik_b l_n}\right\};$$

$$U_{21} = \frac{\omega R_{Ln}}{2k_b\left(s_n l_n + R_{Ln}\right)A_n g}\left(e^{-ik_b l_n} - e^{ik_b l_n}\right);$$

$$U_{22} = \frac{1}{2ik_b\left(s_n l_n + R_{Ln}\right)}\left[\left(ik_b R_{Ln} + s_n\right)e^{ik_b l_n} + \left(ik_b R_{Ln} - s_n\right)e^{-ik_b l_n}\right].$$

Note that the uniform blockage is a special case of the non-uniform blockage when the slope s_n equals to zero ($s_n = 0$). As a result, Eq. (16) becomes

$$\begin{pmatrix} q \\ h \end{pmatrix}_{n+1} = \begin{pmatrix} \cos\left(k_0 l_n\right) & -i\frac{1}{M_{n+1}}\sin\left(k_0 l_n\right) \\ -iM_n \sin\left(k_0 l_n\right) & \cos\left(k_0 l_n\right) \end{pmatrix}\begin{pmatrix} q \\ h \end{pmatrix}_n, \tag{17}$$

where k_0 = wave number for the uniform blockage; $M_n = a/A_n g$. This result is consistent with the transfer matrix for a uniform blockage in Chaudhry (2014).

To study the transient frequency responses, the derived transfer matrix is applied to a reservoir-pipeline-valve (RPV) system as shown in Fig. 3. The transfer matrix with external head and discharge perturbations should be expanded to a 3 × 3 matrix in the following form (Chaudhry, 2014; Duan et al., 2012; Lee et al., 2008b)

$$\begin{pmatrix} q \\ h \\ 1 \end{pmatrix}_B = \begin{pmatrix} U_{11} & U_{12} & U_{13} \\ U_{21} & U_{22} & U_{23} \\ U_{31} & U_{32} & U_{33} \end{pmatrix}\begin{pmatrix} q \\ h \\ 1 \end{pmatrix}_A, \tag{18}$$

where subscripts A and B are upstream and downstream boundaries of the pipeline system. Variables q_B and h_B at the downstream valve can be expressed as

$$q_B = U_{11}q_A + U_{12}h_A + U_{13}, \tag{19}$$

$$h_B = U_{21}q_A + U_{22}h_A + U_{23}. \tag{20}$$

For the RPV system in Fig. 3, it has the boundary conditions $h_A = q_B = 0$. Eqs. (19) and (20) result in

$$h_B = -\frac{U_{21}U_{13}}{U_{11}} + U_{13}. \tag{21}$$

As a result, for a leak-free pipeline system, Eq. (21) becomes (Lee et al., 2006)

$$h_B = -\frac{U_{21}}{U_{11}}. \tag{22}$$

The resonant frequency of head responses for RPV systems with a single non-uniform blockage can be obtained when the denominator of Eq. (22) (i.e., U_{11}) equals to zero.

For RPV systems with a single uniform blockage, (n = 1 and s_1 = 0), the resonance frequency is

$$U_{11} = \cos(k_0 l_1) = 0, \tag{23}$$

which shows that the resonant peaks are uniformly distributed in the frequency domain.

Similarly, for RPV systems with a single non-uniform blockage, (n = 1 and $s_1 \neq 0$), let U_{11} = 0, resulting in the resonant frequency for this RPV system

$$k_b\left(s_1 l_1 + R_{L1}\right)\cos\left(k_b l_1\right) - s_1 \sin\left(k_b l_1\right) = 0. \tag{24}$$

Unlike the resonant frequency for the uniform blockage, Eq. (24) has an extra term $\sin(k_b l_1)$, which may result in resonant frequency shifts. If the slope of this non-uniform blockage equals to 0 (i.e., s_1 = 0), the non-uniform blockage becomes a uniform blockage and Eq. (24) becomes $\cos(k_b l_1) = 0$. This result indicates that resonant peaks for a uniform blockage are uniformly distributed regardless of the radius size, which is consistent with Eq. (23).

The transient frequency responses for a RPV system are studied for both uniform and non-uniform blockages. Note that the friction is neglected herein for highlighting the effect of blockage non-uniformity. As shown in Fig. 3, there is a single blockage (uniform or non-uniform) between the upstream reservoir and downstream valve. The transient wave is caused by the fast and full closure of the downstream valve.

The frequency responses for both cases are plotted in Fig. 4. The frequency is normalized by the fundamental frequency of the pipeline system $\omega_{th} = \bar{a}_b/4l_1$, and is expressed as non-dimensional frequency ω^*. Theoretically the amplitude of head response should go to infinity because the friction is not included in the transfer matrix. It is shown in Fig. 4 that the resonant peaks for the uniform blockage are uniformly distributed, while that for the non-uniform blockage has evident frequency shifts, especially for the first resonant peak. Moreover, as the frequency increases, the induced frequency shift by the non-uniform blockage becomes less evident. This can be explained by the analytical resonant frequency in Eq. (24): as frequency increases, the wave number k_b also increases, then the first term $\cos(k_b l_1)$ in Eq. (24) will become dominant, therefore the frequency shift caused by the non-uniform blockage becomes less evident for higher frequency modes.

Extended transfer matrix for pipeline systems with multiple non-uniform blockages

So far, the transfer matrixes for single uniform and non-uniform blockages have been obtained. For illustration and simplification, only the case of two joint non-uniform blockages shown in Fig. 5(b) is considered and investigated in this study, while for more complex cases similar analysis procedure presented herein can be applied. It is assumed there are no pressure head loss at pipe junctions (Duan et al., 2012). The overall matrix for this pipeline system (made up of four segments), relates the state vectors at two boundaries *A* and *B*, and can be obtained by multiplying individual matrixes for each pipe element in the order of their locations starting from the downstream end.

$$\begin{Bmatrix} q \\ h \end{Bmatrix}_B = \begin{bmatrix} \cos(k_0 l_4) & -i\frac{1}{M_4}\sin(k_0 l_4) \\ -iM_4 \sin(k_0 l_4) & \cos(k_0 l_4) \end{bmatrix} \times \begin{bmatrix} U_{11} & U_{12} \\ U_{21} & U_{22} \end{bmatrix}_3 \times \begin{bmatrix} U_{11} & U_{12} \\ U_{21} & U_{22} \end{bmatrix}_2 \times \begin{bmatrix} \cos(k_0 l_1) & -i\frac{1}{M_1}\sin(k_0 l_1) \\ -iM_1 \sin(k_0 l_1) & \cos(k_0 l_1) \end{bmatrix} \begin{Bmatrix} q \\ h \end{Bmatrix}_A . \quad (25)$$

For clarity, Eq. (25) can be further derived and written as

$$\begin{Bmatrix} q \\ h \end{Bmatrix}_B = \begin{bmatrix} U_{11}^* & U_{12}^* \\ U_{21}^* & U_{22}^* \end{bmatrix} \begin{Bmatrix} q \\ h \end{Bmatrix}_A , \quad (26)$$

where U_{ij}^* = elements of the overall transfer matrix for the four-pipeline system.

Similar with Eqs. (23) and (24), the resonance frequency for the four-pipeline system can be obtained by letting

$$U_{11}^* = 0 \quad (27)$$

Note that the analytical result in Eq. (27) for resonant frequency of a four-pipeline system becomes complicated in its mathematical expression, which can be obtained by solving the former Eqs. (16) and (25). Compared with the intact PRV system, the resonant frequency shift of Eq. (27) can be attributed to two sources: (i) the blockage non-uniformity $A(x)$; (ii) the wave speed non-uniformity $a(x)$ along the axial direction of the PRV system. To highlight the influence of blockage non-uniformity (or to eliminate the influence of wave speed non-uniformity) on resonant frequency shifts and simplify the analytical derivation in Eq. (27), it is first assumed herein that the wave speed in the whole pipeline system is constant, and the absolute values of non-uniform blockage slope $|s_2|$ (constriction section) and $|s_3|$ (expansion section) in Fig. 5(b) are equal ($|s_2| = |s_3| = s$). Then, Eq. (27) becomes

$$4R^2 R_{L3}\omega^3 \cos\left[k_b\left(l_1 + l_2 + l_3 + l_4\right)\right] + \sum a^f s^f \omega^{3-f} F^{3-f}\left(R, R_{L3}\right) \sin\left[k_b\left(l_1 \pm l_2 \pm l_3 \pm l_4\right)\right] = 0 \quad (28)$$

where the second term on the left-hand side contains a series of trigonometric terms; $F()$ = a linear function of R and R_{L3}; f = an integer ranges from 1 to 3. Three special cases are firstly verified as follows:

(1) $s = 0$ (i.e., blockage-free case): the pipe radius on the left boundary of second pipeline in Fig. 5(b) R_{L2} is the same with the intact pipe radius R, $s = 0$ means that there is no blockage in the four-pipeline system. All terms containing s equal zero, and only one term $4R^2R_{L3}\omega^3\cos[k_b(l_1 + l_2 + l_3$

323 $+ l_4)] = 0$ does not contain s. Under this condition, Eq. (28) is simplified into

324 $$\cos[k_b(l_1 + l_2 + l_3 + l_4)] = 0,$$

325 which implies that the resonant peaks for the intact four-pipeline system of Fig. 5(b) are uniformly
326 distributed in the frequency domain, which is consistent with previous studies (Chaudhry, 2014; Lee
327 et al., 2013).

328 (2) $s \sim \infty$ ($(l_2 + l_3)/(l_1 + l_2 + l_3 + l_4) \sim 0$, i.e., discrete blockage case): if the slope of the
329 non-uniform blockage tends to infinity, it means that the length of the non-uniform blockage is
330 negligibly small compared with the total length of the pipeline $(l_2 + l_3)/(l_1 + l_2 + l_3 + l_4) \sim 0$, and the
331 non-uniform blockage can be regarded as a discrete blockage. Terms with s to the high order will
332 become dominant, but the summation of all terms containing s^3 equals to zero. Therefore, all terms
333 containing s^2 are further summed, it turns out to be

334 $$\cos[k_b(l_1 + l_4)] = 0.$$

335 Since the blockage length $l_2 + l_3$ is negligibly small compared with the total length of the pipeline $l_1 +$
336 $l_2 + l_3 + l_4$, the above equation can be approximated by $\cos[k_b(l_1 + l_2 + l_3 + l_4)] = 0$. This is equivalent
337 to the former results for blockage-free case ($s = 0$), and indicates that the discrete blockage does not
338 induce frequency shifts, which is well verified by the known results from previous studies (Lee et al.,
339 2008a, 2013).

340 (3) high frequency harmonic waves: the terms in the equation with the highest order of ω will
341 play dominant roles. Only the term $4R^2R_{L3}\omega^3\cos[k_b(l_1 + l_2 + l_3 + l_4)] = 0$ contains ω^3, therefore Eq. (28)
342 is simplified into

343 $$\cos[k_b(l_1 + l_2 + l_3 + l_4)] = 0,$$

344 which is the same with the blockage-free case ($s = 0$). It means that the frequency shift induced by the

345 blockage non-uniformity becomes less evident as the frequency increases. It is a reminder that this
346 result and analysis here is obtained under the condition of constant wave speed in the whole pipeline
347 system, and the influence of wave speed variation from the blockage section is inspected in the
348 following study.
349
350 **Numerical Validation**
351 To validate the analytical resonant frequency in Eq. (27), the classical frictionless 1D water hammer
352 model coupling with the MOC is adopted herein for comparison. The RPV system with two joint
353 non-uniform blockages is used for the numerical validation. In this study, non-uniform blockages are
354 represented by stainless-steel pipelines with linearly varying diameters as shown in Fig. 5(b). The
355 original intact stainless-steel pipeline (R = 0.25 m, L = 1000 m) is blocked by non-uniform blockages
356 with minimum radius R_{L3} = 0.15 m and $l_2 = l_3$ = 105 m (detailed parameters can refer to Table 2).
357 Wave speeds for intact and blocked pipe sections are calculated based on the wave speed formula
358 given in Wylie et al. (1993) and Chaudhry (2014) as a_0 = 1206 m/s and $\bar{a}_b$ = 1249 m/s. For simplicity
359 of MOC calculation, a_0 and $\bar{a}_b$ are taken to be 1000 m/s and 1050m/s, respectively. In the numerical
360 simulation, the non-uniform blockage is approximated by stepwise discretized grids, and the
361 1000-meter-long pipeline is divided into 3,960 relatively small reaches (i.e., spatial grid size $\Delta x \sim$
362 0.25 m) to decrease the frequency shift caused by numerical errors. The transient (pressure wave) is
363 generated by a sudden and full closure of the downstream valve, and the pressure head trace is
364 measured at the upstream face of the valve. The measured pressure head trace is transformed into the
365 frequency domain by a Fast Fourier transform (FFT) algorithm.
366 The analytical and numerical transient frequency responses with the first 10 resonant peaks are

plotted in Fig. 6(a). In addition, the resonant frequency difference between analytical and numerical MOC results for the first 100 resonant peaks are extracted and plotted in Fig. 6(b). Fig. 6(a) shows that the resonant peaks for the non-uniform blockage system are not uniformly distributed, and this means the presence of the non-uniform blockages has changed the resonant frequencies of the original intact system. Moreover, these figures indicate good agreement between the analytical and numerical results in terms of resonant frequency, which confirms the validity of the analytical result in Eq. (27).

Further Application and Results Analysis

Based on the validated overall transfer matrix, the transient frequency responses for RPV systems with non-uniform blockages, as shown in Fig. 5(b), are investigated in this section. Duan et al. (2012) demonstrated that friction effects (both steady and unsteady) induce decreases in the magnitude of resonant peaks but have little impact on the location of resonant peaks, and the main purpose of this study is to investigate the influence of blockage non-uniformity on resonant frequency shifts. Thus, only the linearized steady friction is included in the following numerical applications. The non-linear steady friction and unsteady friction (Meniconi et al., 2014) can be also included using a similar method as the one presented in Duan et al. (2018).

Uniform and non-uniform blockages with same blocked volume

To study the influence of blockage non-uniformity (blockage severity, length and slope) on transient frequency responses, seven test cases (Tests T1 ~ T7) with different parameters listed in Table 3 are investigated by the analytical results obtained in this study. In this section, the first three tests in Table 3 (i.e., T1 ~ T3) are used for comparison of the impacts of pipe blockage and its non-uniformity on

389 transient frequency responses. Specifically, Tests T2 and T3 are the cases of uniform and non-uniform
390 blockages with same blocked volume in the pipeline, and Test T1 is the intact pipeline system.

391 The transient frequency responses at downstream end for these three tests are plotted in Fig. 7.
392 Fig. 7(a) is shown for the relatively low frequency domain, in which the dimensionless frequency ω^*
393 ranges from 0 to 20. As shown in Fig. 7(a), the resonant peaks for the intact pipeline system are
394 uniformly distributed in the frequency domain, while the presence of uniform and non-uniform
395 blockages within the pipeline results in evident resonant frequency shifts and peak amplitude changes.
396 Moreover, the resonant frequency shift and the peak amplitude change induced by uniform and
397 non-uniform blockages have significant differences, although the same blockage volume has been
398 imposed for the two blockage situations. Fig. 7(b) is plotted for the relatively higher frequency
399 domain, with the dimensionless frequency ω^* from 180 to 200. Similar with low frequency modes,
400 both the resonant frequency shift and peak amplitude change caused by the non-uniform blockage are
401 very different from that caused by the uniform blockage. Nevertheless, the resonant frequency for the
402 non-uniform blockage system almost coincides with that of the blockage-free system. This can be
403 explained by the Special Case (3) of Eq. (28): the frequency shift induced by the non-uniform
404 blockage becomes less evident for high resonant frequency.

405 To gain an insight into the blockage induced frequency shift and amplitude change, the first 100
406 resonant peaks for the uniform and non-uniform blockage systems are further extracted and analyzed.
407 The frequency shifts for uniform and non-uniform blockages are plotted in Fig. 8(a). Note that the
408 blockage induced frequency shift for the m-th resonant peak is defined as $\delta\omega^*_m = \omega^*_{mb} - \omega^*_{mi}$, where
409 ω^*_{mb} = frequency of m-th resonant peak for the blocked pipeline system; and ω^*_{mi} = frequency of m-th
410 resonant peak for the intact pipeline system. It can be observed from Fig. 8(a) that both the uniform

411 and non-uniform blockages induced resonant frequency shifts that fluctuate with the peak number
412 (equivalent to frequency). Specifically, the frequency shift fluctuation induced by the uniform
413 blockage almost keeps the same order of magnitude as the peak number increases, while that induced
414 by the non-uniform blockage is highly frequency-dependent. In the results of non-uniform blockage,
415 the frequency shift fluctuation becomes less evident (tends to zero) as frequency increases. Similarly,
416 the blockage induced resonant peak amplitude change for the m-th resonant peak is defined as $\delta h_{B,m}$ =
417 $h_{B,mb} - h_{B,mi}$, where $h_{B,mb}$ = amplitude of m-th resonant peak for the blocked pipeline system; and $h_{B,mi}$
418 = amplitude of m-th resonant peak for the intact pipeline system. The resonant peak amplitude
419 changes for uniform and non-uniform blockages are plotted in Fig. 8(b) for convenient comparison.
420 Similar with frequency shift fluctuation, the resonant peak amplitude change fluctuation induced by
421 the uniform blockage almost keeps the same order of magnitude, while that induced by the
422 non-uniform blockage gradually decreases with frequency.
423
424 ***Influence of non-uniform blockage severity***
425 In this section, the influence of non-uniform blockage severity on transient frequency responses is
426 investigated. As shown in Fig. 5(b), the length of the non-uniform blockage (l_2 and l_3) is fixed. The
427 blockage severity is defined as $S = (R - R_{L3})/R$, and it is proportional to the slope s of the non-uniform
428 blockage $S \sim s = (R - R_{L3})/l_3$. For tests T3 ~ T5 as shown in Table 3, R_{L3} gradually increases from 0.15
429 to 0.2 m, which means that the non-uniform blockage becomes less severe. The resonant frequency
430 shift and peak amplitude change induced by non-uniform blockages are plotted in Fig. 9. It can be
431 seen from Fig. 9(a) that the overall trend of frequency shift fluctuation for these cases is similar with
432 Test T3 except for the extent of fluctuation. Specifically, the frequency shift fluctuation becomes less

433 evident as the non-uniform blockage becomes less severe. Similarly, Fig. 9(b) shows that the extent of
434 amplitude change fluctuation decreases as the non-uniform blockage becomes less severe. These
435 results are reasonable as severer non-uniform blockage should have more influences on the frequency
436 and amplitude of transient frequency responses for original intact pipeline system. In addition, the
437 overall patterns (or trends) for frequency shift and amplitude change of these three cases are similar.
438 This may indicate that the patterns of frequency shift and amplitude change are independent of the
439 non-uniform blockage severity.
440
441 ***Influence of non-uniform blockage length***
442 The influence of non-uniform blockage length on transient frequency responses is examined herein by
443 fixing other parameters. As is shown in Fig. 5(b), the location of non-uniform blockage center ($l_1 + l_2$)
444 and the pipe radius at the left boundary of Pipe 3 (R_{L3}) are fixed. The non-uniform blockage length (l_2
445 and l_3) gradually decrease from 100 m to 1 m for Tests T3, T6 and T7 in Table 3. It is found that the
446 frequency shift and amplitude change are in certain pattern, and the period of this pattern is inversely
447 proportional to the length of the non-uniform blockage. For convenient observation, the peak number
448 m is divided by the normalized parameter L/l_2, and is expressed as m^* in Fig. 10.
449 Fig. 10(a) shows that the frequency shift patterns for three cases are periodic and roughly the
450 same, meanwhile the period of this induced pattern is in unit length of m^*. The overall extent of the
451 frequency shift periodically decreases in terms of m^*. This frequency shift pattern can be explained by
452 the former Special Case (3) of Eq. (28). As the m^*, which is proportional to ω, increase, the term
453 $4R^2R_{L3}\omega^3\cos[k_b(l_1 + l_2 + l_3 + l_4)]$ containing ω^3 gradually becomes dominant and the frequency shift
454 becomes less evident, thus the overall extent of periodic pattern gradually decrease. In addition, the

455 periodic pattern can be attributed to the remaining trigonometric terms of Eq. (28). Similar behavior
456 can be found in Fig. 10(b) for the amplitude change induced by the non-uniform blockage. Besides,
457 longer non-uniform blockage causes more amplitude attenuation.
458
459 ***Sensitivity analysis of resonant frequency shifts to the wave speed***
460 In realistic pipelines as shown in Fig. 1(a), the wave speed $a_b(x)$ within the non-uniform blockage
461 section would change along the axial direction due to the variation of pipe properties. In the above
462 analytical derivations, the $a_b(x)$ is represented approximately by the average wave speed $\bar{a}_b$ under the
463 same blocked volume condition. As a result, the observed resonant frequency shifts in Tests T3 ~ T7
464 are obtained based on this average wave speed $\bar{a}_b$. Therefore, it is necessary to examine the influence
465 and validity range of this assumption for all tests in this study. For this purpose, the first-order
466 second-moment (FOSM) method (Duan, 2016) is adopted to theoretically investigate the sensitivity of
467 the obtained resonant frequency shift patterns by the developed method in this study to the varying
468 wave speed with average value of $\bar{a}_b$ in the non-uniform blockage section. Eq. (27) describes the
469 relationship between the resonant frequency (ω_m) and system properties (e.g., average wave speed in
470 the blocked section $\bar{a}_b$, wave speed in the intact section a_0, and slope of the non-uniform blockage s),
471 which can be expressed as the following function,

472 $$\omega_m = G\left(\bar{a}_b, a_0, s, R, R_{L3}, l_2, ...\right) = G\left(X_1, X_2, X_3, ..., X_j\right), \quad (29)$$

473 where $G()$ = function; $X_1 - X_j$ = uncertainty factors; j = number of uncertainty factors. The detailed
474 procedures of FOSM for the sensitivity analysis may refer to the previous study of Duan (2016).
475 For quantitative analysis, the sensitivity coefficient of resonant frequency shifts to the average
476 wave speed $\bar{a}_b$ for the m-th resonant peak is defined as the variation (or variation percentage) of the

477 transient response frequency shift to the variation (or variation percentage) of the wave speed

478 $$c_m = \frac{d\left(\delta\omega_m^*\right)}{da_b^*} = \frac{d\left(\delta\omega_m / \omega_{th}\right)}{d\left(a_b / \bar{a}_b\right)}, \quad (30)$$

479 Eq. (30) is evaluated at (μ_1, μ_2, μ_3, …, μ_j), in which $\mu_1 - \mu_j$ are mean values of variables $X_1 - X_j$.

480 By combining the results of Eq. (27) through Eq. (30), the sensitivity coefficients (c_m) of Tests T3,
481 T4, and T5 for the first 100 resonant peaks (representing for both low and relatively high frequency
482 domains) are calculated and plotted in Fig. 11(a). It can be observed in Fig. 11(a) that the first 20
483 resonant peaks (i.e., relatively low frequency domain), which are usually of practical importance, is
484 less sensitive to the wave speed variation compared with remaining resonant peaks in high frequency
485 regions; and the maximum value of sensitivity coefficient (i.e., 0.55) for the first 20 resonant peaks
486 occurs at m = 3 for Test T5. Then, the sensitivity coefficients for two severer blockage cases (i.e.,
487 Tests T3 and T4) gradually increase with frequency. The maximum value of sensitivity coefficient
488 (i.e., 1.01) occurs at m = 97 for Test T3, which means that the maximum error (or uncertainty) of
489 resonant frequency shifts induced by the varying wave speed is in the same order as the variation of
490 wave speed parameter. While the sensitivity coefficients for the shallow blockage case (i.e., Test T5)
491 almost keep the same order of magnitude in the frequency domain, which is much less than 1.0. As a
492 result, the percentage errors of frequency shifts $\Delta\delta\omega^*_m$ induced by the varying wave speed in the
493 blockage section for Tests T3, T4, and T5 are calculated as $\Delta\delta\omega^*_m = c_m((a_0 - \bar{a}_b)/\bar{a}_b)\times 100\%$ and
494 plotted in Fig. 11(b). The result clearly shows that the maximum frequency shift errors for Tests T3,
495 T4, and T5 are within 3.5%, 2.2%, and 1.0%, respectively, which are acceptable for the blockage
496 detection application in this study.

497

498 **Discussion and Implication**

499 The above results and analysis suggest that, unlike the uniform blockage, the frequency shift $\delta\omega^*_m$
500 induced by the non-uniform blockage is frequency dependent, $\delta\omega^*_m \sim 1/\omega^*_m$. As the frequency ω^*_m
501 increases, the induced frequency shift $\delta\omega^*_m$ becomes less evident. This finding is useful to explain the
502 inaccuracy of the current frequency domain TBBDM, which is based on the blockage induced
503 frequency shift, for non-uniform blockages detection in Duan et al. (2017). Therefore, further
504 improvement of such transient-based method is necessary for the non-uniform blockage detection.

505 The results comparison has also shown that, with fixed blockage length, the blockage induced
506 frequency shift gets more evident as the non-uniform becomes severer (i.e., $\delta\omega^*_m \sim s$). Besides, the
507 overall extent of frequency shifts for different blockage severities is decreased as frequency increases
508 (i.e., $\delta\omega^*_m \sim 1/\omega^*_m$). Therefore, for fixed blockage length, the blockage induced frequency shift $\delta\omega^*_m$
509 is proportional to the slope of the non-uniform blockage (s), and is inversely related to the frequency
510 ω^*_m, that is $\delta\omega^*_m \sim s/\omega^*_m$. In addition, for fixed blockage severity, the frequency shift pattern for
511 various blockage length is the same, and the period of this pattern $T_{pattern}$ is inversely proportional to
512 the length of the blockage $T_{pattern} \sim 1/l_2$. This period may offer us a method to detect the length of the
513 non-uniform blockage. Based on $m/(L/l_2) = T(m^*)$, where $T = 1$ is the period of the frequency shift
514 pattern in terms of m^*, the blockage length l_2 can be determined.

515 The obtained dependence relationship of transient wave behavior and blockage non-uniformity
516 may provide useful implication to the transient analysis and blockage detection in real pipeline
517 systems. Specifically, the current TBBDM can be further extended to more general and realistic
518 situations of pipe blockages. That is, it is necessary to include the characteristic parameters, i.e., the
519 slope (s), severity (R_{L3}) and location (l_4) of non-uniform blockages, in the TBBDM, which can be
520 inversely determined based on the derived results of Eq. (27) in this study. Consequently, it is

521 expected that, based on the results and findings of this study, the accuracy of current transient-based
522 method can be improved and extended for realistic pipeline diagnosis, which will be investigated
523 through further theoretical analysis and experimental tests in the next-step work.

524 It is worthy of noting that the wave equation, Eq. (1), used in this research is derived based on
525 the classic 1D water hammer model where the plane wave assumption has been imposed (Chaudhry,
526 2014). As a result, the validity frequency range of this wave equation will be governed by the plane
527 wave condition. According to previous studies on radial pressure waves (Che et al., 2018; Hall, 1932;
528 Louati & Ghidaoui, 2017), the plane wave assumption is valid only when the harmonic frequencies
529 are lower than the cut-off frequency of given pipe systems. On this point, all the peak frequencies
530 used for analysis in this study are much smaller than this critical cut-off frequency of the blocked pipe
531 systems. In other words, the used 1D wave equation is valid for all the results obtained in the present
532 study. In addition, the average wave speed within non-uniform blockages in Table 3 is mainly
533 evaluated from the changes of pipe diameters due to blockages. This is mainly because the main
534 purpose of this study is to examine the influence of blockage non-uniformity on transient frequency
535 responses. However, the developed method of this study is still valid for practical applications where
536 the wave speed varies with different factors, such as pipe diameters, wall thickness, and modulus of
537 elasticity of the pipe wall, only if such information is known to the models.

538

539 **Conclusions**

540 This paper investigates the transient frequency responses for pressurized water pipeline systems with
541 non-uniform blockages. The transient wave behavior is obtained by analytically solving the wave
542 equation for a single blockage with a linearly varying diameter. The wave solution is used to derive

543 the overall transfer matrix for a pressurized water pipeline system with non-uniform blockages, which
544 is then numerically validated by the traditional MOC. With validated analytical results, the influences
545 of blockage shape (slope), severity and length on transient frequency responses are studied
546 systematically for different cases. The results indicate the non-uniform blockage may induce very
547 different modification patterns on the frequency shift and amplitude change of transient waves from
548 the uniform blockage situation. The findings of this study are useful to improve the current
549 transient-based method for non-uniform blockage detection in real pipeline systems. Although only
550 the linear geometry of the non-uniform blockages has been considered in current study, this research
551 may provide a framework for exploring the diagnosis and analysis of realistic pipelines with
552 non-uniform blockages. It is also noted that more investigations including numerical and experimental
553 tests are required in the future work.
554
555 **Acknowledgements**
556 This research work was supported by the research grants from: (1) the Hong Kong Research Grants
557 Council (projects no. T21-602/15-R, no. 25200616 and no. 15201017); and (2) the Hong Kong
558 Polytechnic University (projects no. 1-ZVCD and no. 1-ZVGF).
559
560 **Notation**
561 $A = A(x)$ = pipe cross-sectional area (m^2)
562 $a = a(x)$ = wave speed ($m\ s^{-1}$)
563 a_0 = wave speed in intact pipelines ($m\ s^{-1}$)
564 $a_b = a_b(x)$ = wave speed within non-uniform blockages ($m\ s^{-1}$)

565 $\bar{a}_b$ = average wave speed within non-uniform blockages (m s^{-1})

566 c_m = sensitivity coefficient

567 g = gravitational acceleration (m s^{-2})

568 h = pressure head deviation in the frequency domain (m)

569 $k = k(x) = \omega/a(x)$ = wave number (rad m^{-1})

570 k_b = wave number for the non-uniform blockage (rad m^{-1})

571 k_0 = wave number for the uniform blockage (rad m^{-1})

572 L = total length of pipeline systems (m)

573 l_n = length of the n-th non-uniform blockage (m)

574 m = peak number

575 n = pipeline number

576 P = instantaneous pressure in the time domain (Pa)

577 P_0 = mean pressure in the time domain (Pa)

578 p^* = pressure deviation from the P_0 (Pa)

579 p = pressure in the frequency domain (Pa)

580 q = discharge deviation in the frequency domain (m^3 s^{-1})

581 R = intact pipe radius (m)

582 R_{Ln} = pipe radius at the left boundary of the n-th non-uniform blockage (m)

583 r_n = pipe radius of the n-th non-uniform blockage (m)

584 $S = (R - R_{L3})/R$ = blockage severity

585 $s_n = (R - R_{Ln})/l_n$ = slope of the n-th non-uniform blockage

586 t = time (s)

587 U_{ij} = elements of transfer matrix

588 U_{ij}^* = elements of the overall transfer matrix for the four-pipeline system

589 x = axial coordinate along the pipeline (m)

590 $\delta\omega^*_m$ = blockage induced frequency shift for the m-th resonant peak

591 $\delta h_{B,m}$ = blockage induced resonant peak amplitude change for the m-th resonant peak (m)

592 ω = angular frequency (rad s^{-1})

593 ω_{th} = fundamental frequency of the pipeline system (rad s^{-1})

594 ω^* = non-dimensional frequency

595 ω^*_{mb} = frequency of m-th resonant peak for the blocked pipeline system

596 ω^*_{mi} = frequency of m-th resonant peak for the intact pipeline system

597

598 **References**

599 Brunone, B. (1999). "Transient test-based technique for leak detection in outfall pipes." *J. Water*
600 *Resour. Plann. Manage.,* 10.1061/(ASCE)0733-9496(1999)125:5(302), 302-306.

601 Brunone, B., & Ferrante, M. (2001). "Detecting leaks in pressurised pipes by means of transients." *J.*
602 *Hydraul. Res., 39*(5), 539-547.

603 Brunone, B., & Ferrante, M. (2004). "Pressure waves as a tool for leak detection in closed conduits."
604 *Urban Water J., 1*(2), 145-155.

605 Brunone, B., Ferrante, M., & Meniconi, S. (2008). "Discussion of "detection of partial blockage in
606 single pipelines" by PK Mohapatra, MH Chaudhry, AA Kassem, and J. Moloo." *J. Hydraul. Eng.,*
607 10.1061/(ASCE)0733-9429(2008)134:6(872), 872-874.

608 Chaudhry, M. H. (2014). *Applied hydraulic transients*, 3rd Ed., Springer, New York.

609 Che, T. C., Duan, H. F., Lee, P. J., Meniconi, S., Pan, B., & Brunone, B. (2018). "Radial pressure
610 wave behavior in transient laminar pipe flows under different flow perturbations." *J. Fluids Eng.,*
611 accepted and in press.

612 Colombo, A. F., Lee, P. J., & Karney, B. W. (2009). "A selective literature review of transient-based

613 leak detection methods." *J. Hydro-environ. Res., 2*(4), 212-227.
614 Covas, D., & Ramos, H. (2010). "Case studies of leak detection and location in water pipe systems by
615 inverse transient analysis." *J. Water Resour. Plann. Manage.,*
616 10.1061/(ASCE)0733-9496(2010)136:2(248), 248-257.
617 Covas, D., Ramos, H., Graham, N., & Maksimovic, C. (2004). "Application of hydraulic transients
618 for leak detection in water supply systems." *Water Sci. Tech.: W. Sup., 4*(5-6), 365-374.
619 Datta, S., & Sarkar, S. (2016). "A review on different pipeline fault detection methods." *J. Loss*
620 *Prevent. Proc., 41*(2016), 97-106.
621 Duan, H. F. (2016). "Sensitivity analysis of a transient-based frequency domain method for extended
622 blockage detection in water pipeline systems." *J. Water Resour. Plann. Manage.,*
623 10.1061/(ASCE)WR.1943-5452.0000625, 04015073.
624 Duan, H. F. (2017). "Transient wave scattering and its influence on transient analysis and leak
625 detection in urban water supply systems: theoretical analysis and numerical validation." *Water,*
626 *9*(10), 789.
627 Duan, H. F., Che, T. C., Lee, P. J., & Ghidaoui, M. S. (2018). "Influence of nonlinear turbulent friction
628 on the system frequency response in transient pipe flow modelling and analysis." *J. Hydraul. Res.*,
629 10.1080/00221686.2017.1399936, accepted and online available.
630 Duan, H. F., Lee, P. J., Che, T. C., Ghidaoui, M. S., Karney, B. W., & Kolyshkin, A. A. (2017). "The
631 influence of non-uniform blockages on transient wave behavior and blockage detection in
632 pressurized water pipelines." *J. Hydro-environ. Res.*, *17*(2017), 1-7.
633 Duan, H. F., Lee, P. J., Ghidaoui, M. S., & Tuck, J. (2014). "Transient wave-blockage interaction and
634 extended blockage detection in elastic water pipelines." *J. Fluids Struct., 46*(2014), 2-16.
635 Duan, H. F., Lee, P. J., Ghidaoui, M. S., & Tung, Y. K. (2010). "Essential system response
636 information for transient-based leak detection methods." *J. Hydraul. Res., 48*(5), 650-657.
637 Duan, H. F., Lee, P. J., Ghidaoui, M. S., & Tung, Y. K. (2012). "Extended blockage detection in
638 pipelines by using the system frequency response analysis." *J. Water Resour. Plann. Manage.,*
639 10.1061/(ASCE)WR.1943-5452.0000145, 55-62.
640 Duan, H. F., Lu, J. L., Kolyshkin, A. A., & Ghidaoui, M. S. (2011). "The effect of random
641 inhomogeneities of pipe cross-sectional area on wave propagation." *Proc*., 34*th IAHR Congress*,
642 Brisbane, Australia.

643 Ferrante, M., & Brunone, B. (2003). "Pipe system diagnosis and leak detection by unsteady-state tests.
644 1. Harmonic analysis." *Adv. Water Resour., 26*(1), 95-105.
645 Gong, J., Zecchin, A. C., Simpson, A. R., & Lambert, M. F. (2014). "Frequency response diagram for
646 pipeline leak detection: comparing the odd and even harmonics." *J. Water Resour. Plann. Manage.,*
647 10.1061/(ASCE)WR.1943-5452.0000298, 65-74.
648 Hall, W. M. (1932). "Comments on the theory of horns." *J. Acoust. Soc. Am., 3*(4), 552-561.
649 James, W., & Shahzad, A. (2003). "Water distribution losses caused by encrustation and biofouling:
650 theoretical study applied to Walkerton, ON." *Proc., World Water & Environmental Resources*
651 *Congress* 2003, Pennsylvania, United States.
652 Kim, S. H. (2017). "Multiple leakage function for a simple pipeline system." *Water Resour. Manage.,*
653 *31*(9), 2659–2673.
654 Lee, P. J., Duan, H. F., Ghidaoui, M. S., & Karney, B. W. (2013). "Frequency domain analysis of pipe
655 fluid transient behaviour." *J. Hydraul. Res., 51*(6), 609-622.
656 Lee, P. J., Duan, H. F., Tuck, J., & Ghidaoui, M. S. (2015). "Numerical and experimental study on the
657 effect of signal bandwidth on pipe assessment using fluid transients." *J. Hydraul. Eng.,*
658 10.1061/(ASCE)HY.1943-7900.0000961, 04014074.
659 Lee, P. J., Lambert, M. F., Simpson, A. R., Vítkovský, J. P., & Liggett, J. A. (2006). "Experimental
660 verification of the frequency response method for pipeline leak detection." *J. Hydraul. Res., 44*(5),
661 693-707.
662 Lee, P. J., Tuck, J., Davidson, M., & May, R. (2017). "Piezoelectric wave generation system for
663 condition assessment of field water pipelines." *J. Hydraul. Res., 55*(5), 721-730.
664 Lee, P. J., Vitkovsky, J. P., Lambert, M. F., Simpson, A. R., & Liggett, J. A. (2008a). "Discrete
665 blockage detection in pipelines using the frequency response diagram: Numerical study." *J.*
666 *Hydraul. Eng.,* 10.1061/(ASCE)0733-9429(2008)134:5(658), 658-663.
667 Lee, P. J., Vítkovský, J. P., Lambert, M. F., Simpson, A. R., & Liggett, J. A. (2007). "Leak location in
668 pipelines using the impulse response function." *J. Hydraul. Res., 45*(5), 643-652.
669 Lee, P. J., Vítkovský, J. P., Lambert, M. F., Simpson, A. R., & Liggett, J. A. (2008b). "Discrete
670 blockage detection in pipelines using the frequency response diagram: numerical study." *J.*
671 *Hydraul. Eng.,* 10.1061/(ASCE)0733-9429(2008)134:5(658), 658-663.
672 Louati, M., & Ghidaoui, M. S. (2017). "High-frequency acoustic wave properties in a water-filled

673 pipe. Part 1: dispersion and multi-path behaviour." *J. Hydraul. Res., 55*(5), 613-631.
674 Louati, M., Meniconi, S., Ghidaoui, M. S., & Brunone, B. (2017). "Experimental study of the
675 eigenfrequency shift mechanism in a blocked pipe system." *J. Hydraul. Eng.,*
676 10.1061/(ASCE)HY.1943-7900.0001347, 04017044.
677 Meniconi, S., Brunone, B., & Ferrante, M. (2010). "In-line pipe device checking by short-period
678 analysis of transient tests." *J. Hydraul. Eng.,* 10.1061/(ASCE)HY.1943-7900.0000309, 713-722.
679 Meniconi, S., Brunone, B., Ferrante, M., & Massari, C. (2011). "Small amplitude sharp pressure
680 waves to diagnose pipe systems." *Water Resour. Manage., 25*(1), 79-96.
681 Meniconi, S., Duan, H. F., Brunone, B., Ghidaoui, M. S., Lee, P. J., & Ferrante, M. (2014). "Further
682 developments in rapidly decelerating turbulent pipe flow modeling." *J. Hydraul. Eng.,*
683 10.1061/(ASCE)HY.1943-7900.0000880, 04014028.
684 Meniconi, S., Duan, H. F., Lee, P. J., Brunone, B., Ghidaoui, M. S., & Ferrante, M. (2013).
685 "Experimental investigation of coupled frequency and time-domain transient test–based techniques
686 for partial blockage detection in pipelines." *J. Hydraul. Eng.,*
687 10.1061/(ASCE)HY.1943-7900.0000768, 1033-1040.
688 Munjal, M. L. (2014). *Acoustics of ducts and mufflers*, Wiley.
689 Rubio Scola, I., Besançon, G., & Georges, D. (2017). "Blockage and leak detection and location in
690 pipelines using frequency response optimization." *J. Hydraul. Eng.,*
691 10.1061/(ASCE)HY.1943-7900.0001222, 04016074.
692 Sattar, A. M., & Chaudhry, M. H. (2008). "Leak detection in pipelines by frequency response method."
693 *J. Hydraul. Res., 46*(sup1), 138-151.
694 Sattar, A. M., Chaudhry, M. H., & Kassem, A. A. (2008). "Partial blockage detection in pipelines by
695 frequency response method." *J. Hydraul. Eng.,* 10.1061/(ASCE)0733-9429(2008)134:1(76),
696 76-89.
697 Stephens, M. L. (2008). "Transient response analysis for fault detection and pipeline wall condition
698 assessment in field water transmission and distribution pipelines and networks." Ph.D. thesis, Univ.
699 of Adelaide, Adelaide, Australia.
700 Tuck, J., Lee, P. J., Davidson, M., & Ghidaoui, M. S. (2013). "Analysis of transient signals in simple
701 pipeline systems with an extended blockage." *J. Hydraul. Res., 51*(6), 623-633.
702 Wang, X. J., Lambert, M. F., & Simpson, A. R. (2005). "Detection and location of a partial blockage

in a pipeline using damping of fluid transients." *J. Water Resour. Plann. Manage.*, 10.1061/(ASCE)0733-9496(2005)131:3(244), 244-249.

Webster, A. G. (1919). "Acoustical impedance and the theory of horns and of the phonograph." *Proc. Natl. Acad. Sci., 5*(7), 275-282.

Wylie, E. B., Streeter, V. L., & Suo, L. (1993). *Fluid transients in systems*, Prentice Hall, Englewood Cliffs, NJ.

Figure Captions

Fig. 1. (a) Non-uniform blockages in practical urban water pipelines (James & Shahzad, 2003; Stephens, 2008; Duan et al., 2017); (b) sketch of realistic pipeline with non-uniform blockages; (c) sketch of pipeline with non-uniform blockages used for analytical analysis.

Fig. 2. Transient wave behavior in uniform and non-uniform blockages.

Fig. 3. Illustrative RPV systems with: (a) single uniform blockage; (b) single non-uniform blockage.

Fig. 4. Transient frequency responses for RPV systems with single uniform and non-uniform blockages (without friction effect).

Fig. 5. Illustrative RPV systems with: (a) uniform blockages; (b) non-uniform blockages.

Fig. 6. Comparison of analytical and numerical results without friction effect: (a) transient frequency responses; (b) resonant frequency difference between analytical and numerical MOC results.

Fig. 7. Comparison of transient frequency responses for different pipe blockage situations with linearized steady friction effect: (a) low frequency mode domain; (b) higher frequency mode domain.

Fig. 8. Influence of uniform and non-uniform blockages on transient frequency responses: (a) relative resonant frequency shift; (b) relative resonant peak amplitude change.

Fig. 9. Influence of non-uniform blockage with different blockage severities on transient frequency responses: (a) relative resonant frequency shift; (2) relative resonant peak amplitude change.

Fig. 10. Influence of non-uniform blockage with different blockage lengths on transient frequency responses: (a) relative resonant frequency shift; (b) relative resonant peak amplitude change.

Fig. 11. (a) Sensitivity coefficients of resonant frequency shifts to the average wave speed within the blocked section; (b) errors of resonant frequency shifts for Tests T3, T4, and T5.

Tables

Table 1. Parameter settings for illustrative systems with uniform and non-uniform blockages

Type	l_n	s_n	R_{Ln}	k_b
Uniform blockage	100R	0	0.9R	$\pi/5$
Non-uniform blockage	100R	2e–3	0.8R	$\pi/5$

751

752

753 **Table 2.** Parameter settings for numerical validation

Blockage type	l_1 (m)	l_2 (m)	l_3 (m)	l_4 (m)	R (m)	s	R_{L3} (m)	a_0 (m/s)	$\bar{a}_b$ (m/s)
non-uniform	295	105	105	495	0.25	0.1/105	0.15	1000	1050

754

Table 3. Parameter settings for numerical test systems

Test no.	Blockage type	l_1 (m)	l_2 (m)	l_3 (m)	l_4 (m)	R (m)	s	R_{L3} (m)	a_0 (m/s)	$\bar{a_b}$ (m/s)
T1	blockage-free	300	100	100	500	0.25	0	0.25	1206	1206
T2	uniform	300	100	100	500	0.25	0	0.20	1206	1249
T3	non-uniform	300	100	100	500	0.25	1e-3	0.15	1206	1249
T4	non-uniform	300	100	100	500	0.25	7.5e-4	0.175	1206	1238
T5	non-uniform	300	100	100	500	0.25	5e-4	0.20	1206	1227
T6	non-uniform	390	10	10	590	0.25	1e-2	0.15	1206	1249
T7	non-uniform	399	1	1	599	0.25	1e-1	0.15	1206	1249

Figures

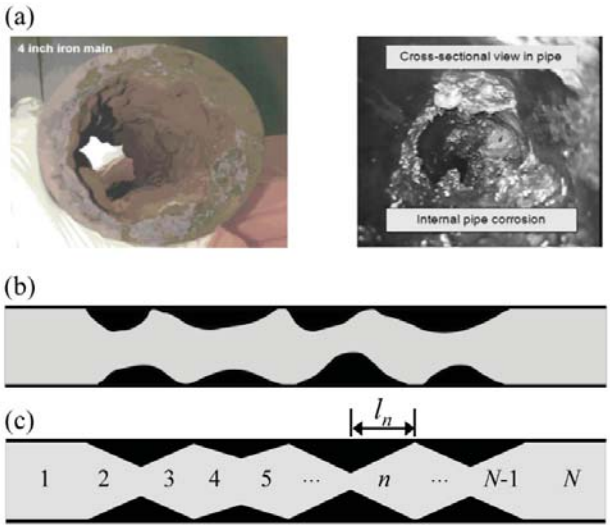

Fig. 1. (a) Non-uniform blockages in practical urban water pipelines (James & Shahzad, 2003; Stephens, 2008; Duan et al., 2017b); (b) sketch of realistic pipeline with non-uniform blockages; (c) sketch of pipeline with non-uniform blockages used for analytical analysis.

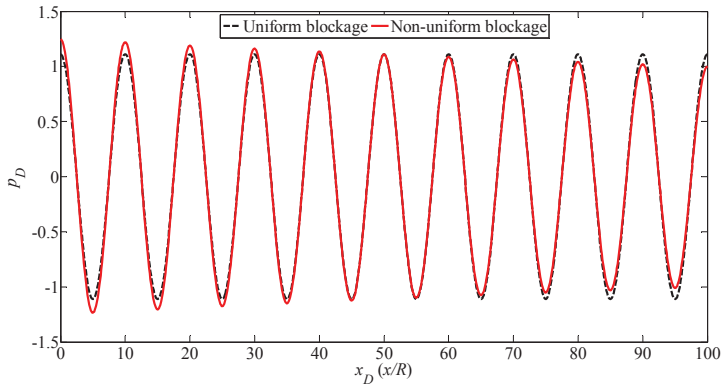

Fig. 2. Transient wave behavior in uniform and non-uniform blockages.

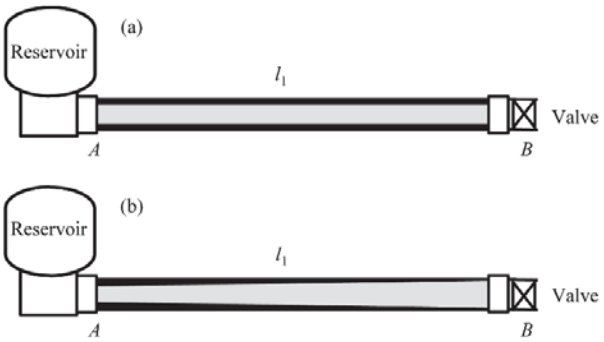

Fig. 3. Illustrative RPV systems with a: (a) single uniform blockage; (b) single non-uniform blockage.

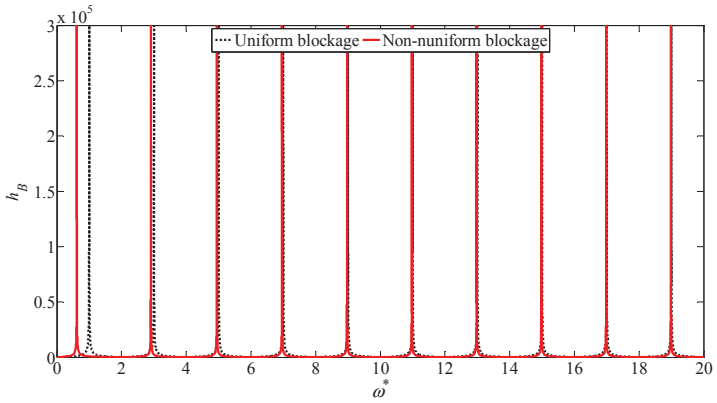

Fig. 4. Transient frequency responses for RPV systems with single uniform and non-uniform blockages (without friction effect).

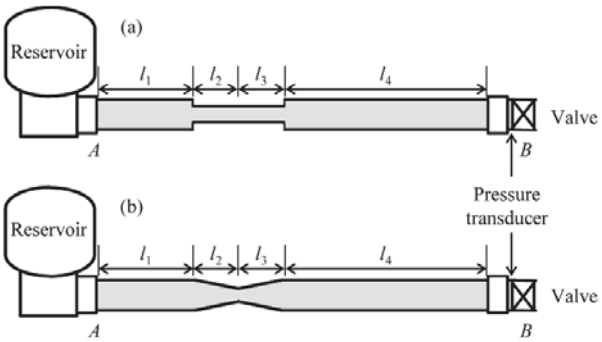

Fig. 5. Illustrative RPV systems with: (a) uniform blockages; (b) non-uniform blockages.

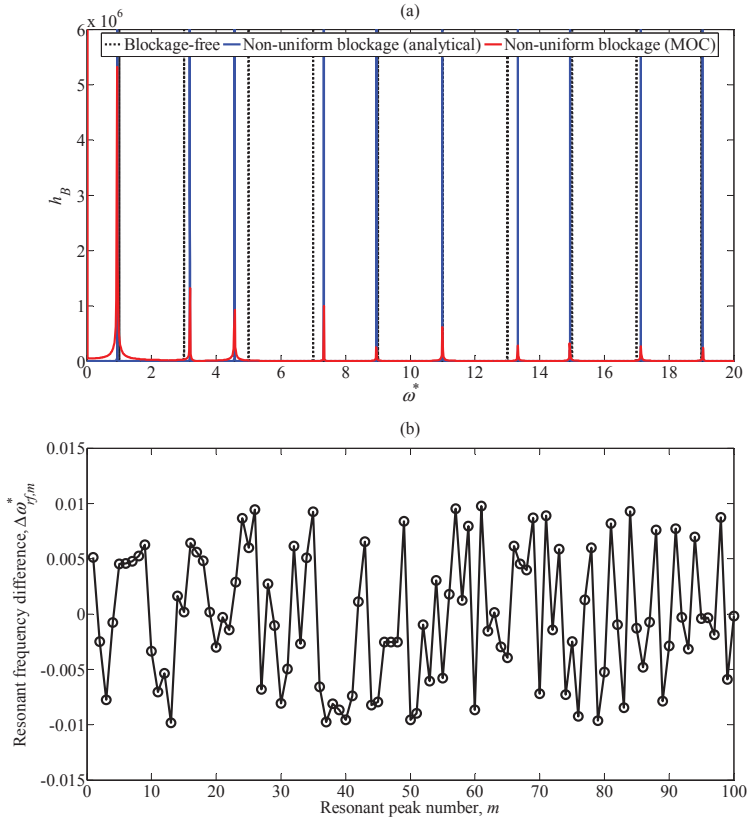

Fig. 6. Comparison of analytical and numerical results without friction effect: (a) transient frequency responses; (b) resonant frequency difference between analytical and numerical MOC results.

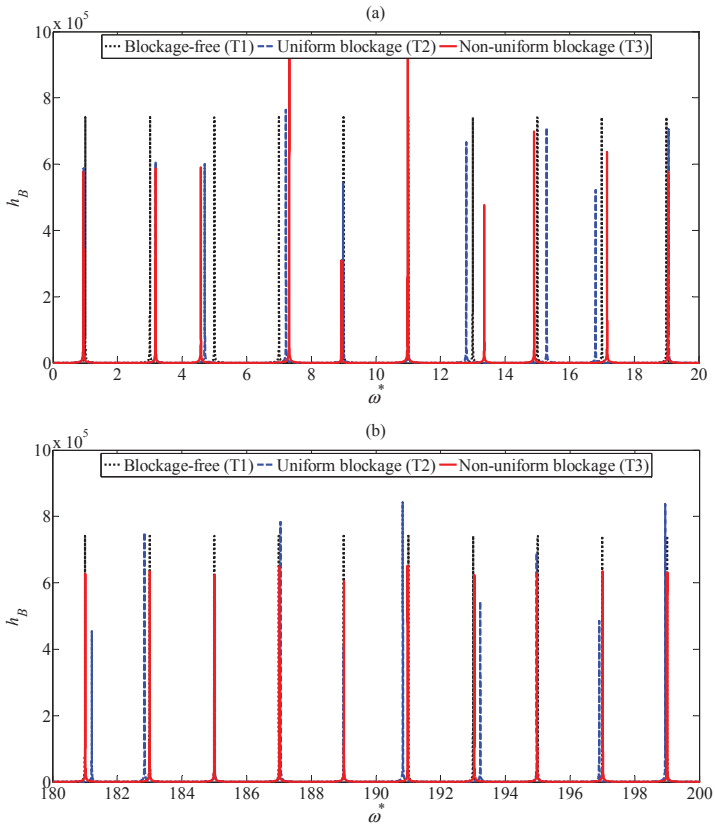

Fig. 7. Comparison of transient frequency responses for different pipe blockage situations with linearized steady friction effect: (a) low frequency mode domain; (b) higher frequency mode domain.

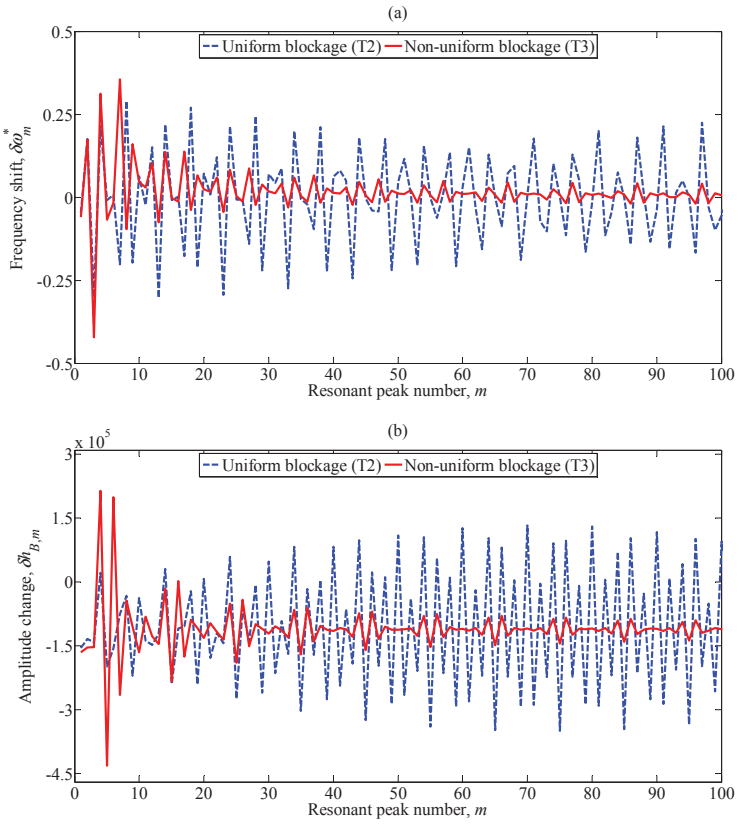

Fig. 8. Influence of uniform and non-uniform blockages on transient frequency responses: (a) relative resonant frequency shift; (b) relative resonant peak amplitude change.

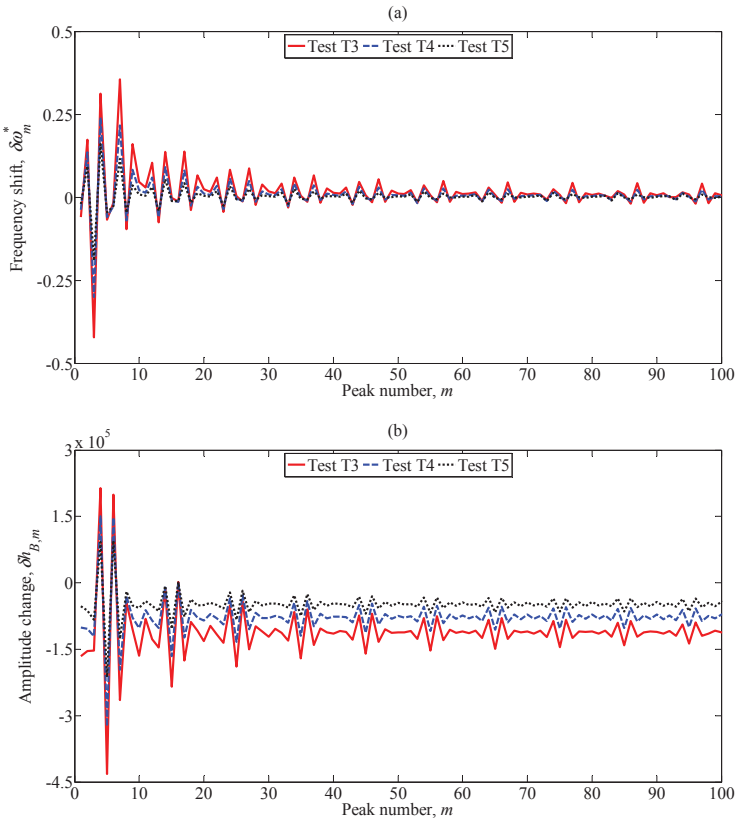

Fig. 9. Influence of non-uniform blockage with different blockage severities on transient frequency responses: (a) relative resonant frequency shift; (2) relative resonant peak amplitude change.

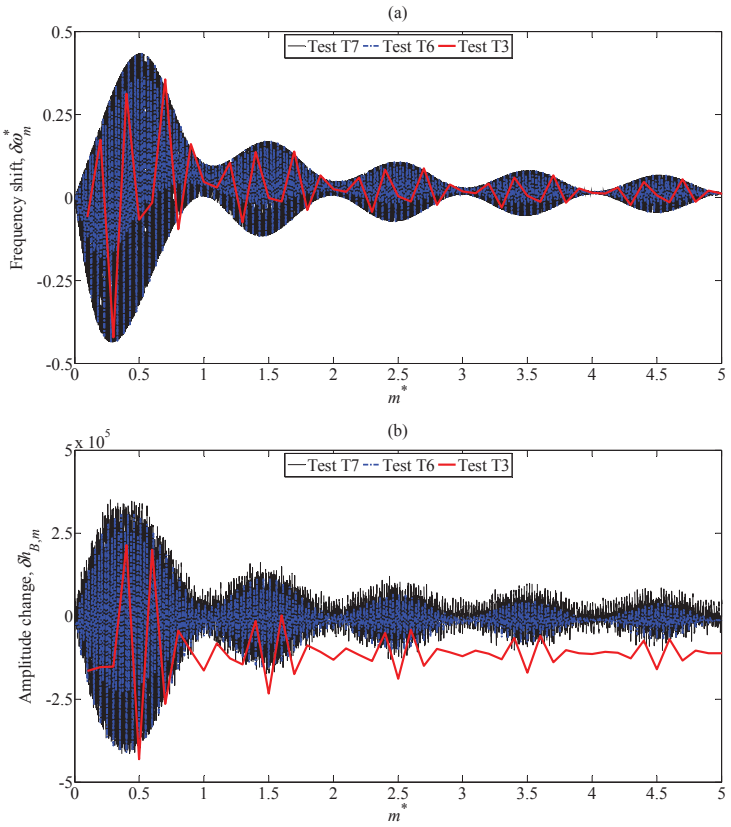

Fig. 10. Influence of non-uniform blockage with different blockage lengths on transient frequency responses: (a) relative resonant frequency shift; (b) relative resonant peak amplitude change.

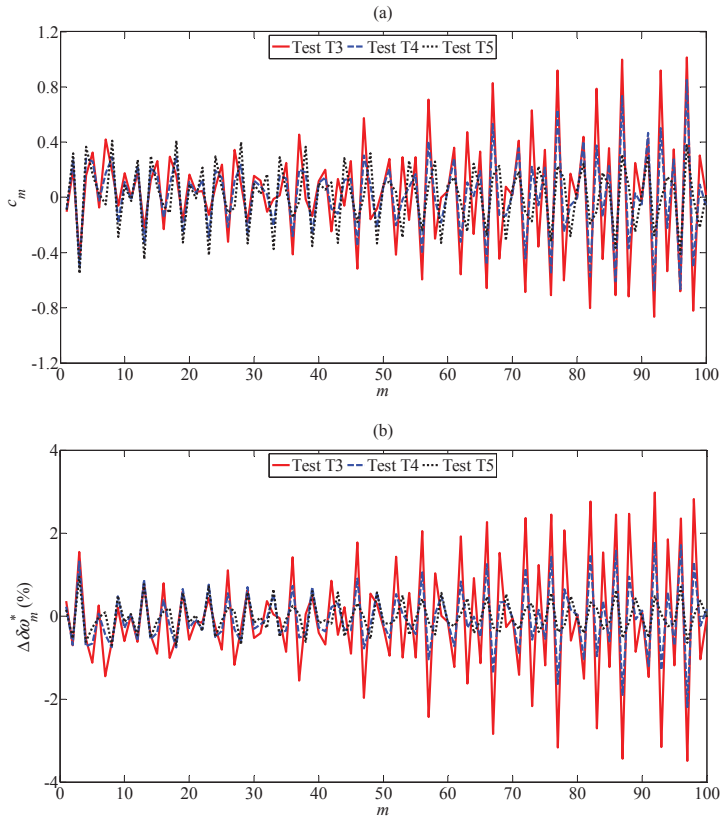

Fig. 11. (a) Sensitivity coefficients of resonant frequency shifts to the average wave speed within the blocked section; (b) errors of resonant frequency shifts for Tests T3, T4, and T5.